Bulgarian Chemical Communications, Volume 56, Issue 3 (pp. 328-332) 2024 DOI: 10.34049/bcc.56.3.OZ-M

The influence of gold nanorods' aspect ratio on the structure and spectroscopic properties of TiO_2 nanoparticles for solar cell utilization

Z. B. Al-Ruqeishi, O. K. Abou-Zied*

Department of Chemistry, College of Science, Sultan Qaboos University, Box 36, Al-Khod 123, Sultanate of Oman

Received May 3, 2024; Accepted: August 15, 2024

In this study, gold nanorods (Au NRs) were employed to modify a TiO_2 semiconductor nanolayer for potential integration into dye-sensitized solar cells (DSSCs)' photoanode, aiming to enhance absorption in the visible to near-infrared (NIR) spectral region and mitigate electron-hole recombination. Two aspect ratios of Au NRs were synthesized and their interaction with TiO_2 was investigated. Both Au NR types show two distinct absorption peaks in the visible to NIR spectral region due to the surface plasmon resonance effect. The aspect ratios of the prepared Au NRs were determined using transmission electron microscopy. X-ray photoelectron spectroscopy measurements indicated electronic charge transfer from TiO_2 nanoparticles (NPs) to Au NRs, evidenced by blue shifts in the Ti 2p and O 1s peaks. Photoluminescence (PL) analysis revealed decreased emission intensity in TiO_2 NPs decorated with Au NRs, which is attributed to a formed Schottky barrier that reduces the electron-hole recombination process by acting as an electron sink. Notably, the PL intensity of TiO_2 NPs decorated with the larger aspect ratio of Au NRs (4.93) is lower, compared to that decorated with the smaller aspect ratio (2.41). This result suggests superior electron trapping and charge carrier separation, leading to reduced electron-hole recombination rates.

Keywords: Au nanorods; TiO_2 nanoparticles; dye-sensitized solar cells.

INTRODUCTION

Titanium dioxide (TiO_2) nanomaterial is considered a highly promising semiconductor in various scientific fields such as photocatalysis, lithium-ion batteries, water splitting, and solar cells due to its unique characteristics [1-4]. Particularly, TiO_2 has attracted the greatest attention as a potential photoanode for dye-sensitized solar cells (DSSCs) because of its large band gap, high surface area for dye adsorption, high chemical stability, lack of toxicity, and fast electron transfer rate [5, 6]. Despite the advantages of TiO_2, it has low electron diffusion coefficients because of defects, surface states, grain boundaries, and other structures that act as electron trapping sites. This results in a decrease in charge-carrier mobility, a decrease in charge-carrier separation lifetime, and an increase in the rate of electron-hole recombination, which subsequently limits the efficiency of DSSCs [7, 8]. The most common approach for suppressing the charge recombination process in TiO_2, is structural modification with metal nanoparticles, non-metals, semiconductor coupling, and hybridization with carbon materials [9-13]. Moreover, the surface plasmon resonance effect (SPR) of plasmonic metal nanostructures provides an enhancement of visible light absorption. The shape of a metal nanostructure has an impact on the performance of DSSCs. In particular, rod-shaped Au nanostructures have a greater photovoltaic efficiency than Au nanoparticles (Au NPs) because they further boost light harvesting in the near-infrared (NIR) spectral region. Furthermore, the Au nanorods (Au NRs) provide higher carrier recombination resistance and faster charge carrier transportation compared to Au NPs [14].

In this study, we modified TiO_2 nanolayers by preparing nanocomposites with Au NRs of varying aspect ratios, aiming at potential application as photoanodes in DSSCs. The morphology and size of the Au NRs were determined through transmission electron microscopy while X-ray photoelectron spectroscopy was utilized to analyze the deposition of Au NRs onto TiO_2 nanomaterial. We observed a substantial enhancement in optical absorption within the visible (Vis) and NIR spectral regions for the new materials. The photoluminescence spectra indicate a large reduction in the electron-hole recombination process as a result of efficient electron trapping. These TiO_2/Au NRs nanocomposites hold promise in enhancing light harvesting from the solar radiation, while facilitating interfacial charge transfer when employed as photoanodes in DSSCs.

* To whom all correspondence should be sent:
E-mail: *abouzied@squ.edu.om*

MATERIALS AND METHODS

Synthesis of Au NRs@TiO_2 nanocomposites

The two aspect ratios of Au NRs were synthesized using a seed-mediated method following the procedure outlined by Feng *et al*. [15]. The aspect ratio was controlled by using different volumes of $AgNO_3$ (50 and 105 µL) in the growth solution. The nanocomposite was prepared by mixing 0.2 g of TiO_2 (P25), 0.4 ml of 24% NH_3, 0.8 ml of mercaptoacetic acid, and 6.8 ml of H_2O. The solution mixture was vigorously stirred for a duration of 24 h. Subsequently, 8 ml of the previously prepared Au NRs was added to the solution and maintained at the same stirring speed for additional 24 h. Purification of the nanocomposite involved removing the mercaptoacetic acid and repeated washing of the precipitate with water. The nanocomposite was then centrifuged for 10 min at a speed of 7,000 rpm, and the resulting precipitate was redispersed in deionized water before being allowed to completely dry at room temperature.

Characterization techniques

The morphology of the prepared samples was examined using field emission transmission electron microscopy (FE-TEM, JEOL JEM-2100F). The optical absorption and photoluminescence properties were determined at room temperature using Agilent 8453 spectrophotometer and Perkin Elmer LS55 fluorescence spectrophotometer, respectively. X-ray photoelectron spectroscopy (XPS) (Scienta Omicron, Germany) utilizing Al-k (hν = 1486.6 eV) at a working voltage of 15 kV under 10^{-8} Pa was employed to investigate the elemental composition.

RESULTS AND DISCUSSION

Absorption spectra of Au NRs

The Vis–NIR absorption spectra of Au NRs were recorded to investigate their optical characteristics. Electronic excitation causes the Au NRs to have two SPR modes [16], transverse SPR (TSPR) due to electron oscillations in the Au NRs' transverse direction, and longitudinal SPR (LSPR) associated with electron oscillations in the Au NRs' longitudinal direction. The former appears as an absorption band in the 510–530 nm region, while the latter absorption peak is modulated from Vis to NIR by changing the aspect ratio [15, 17].

The Vis–NIR absorption spectra of the two different aspect ratios of Au NRs prepared here are displayed in Fig. 1. The terminology in the figure (Au NR (n)) is based on the amount of $AgNO_3$ in the growing solution, where n is the concentration of $AgNO_3$ in micromoles (µM). The Au NRs show significant LSPR bands at 634 nm and 819 nm as the $AgNO_3$ concentration increases, and weak TSPR bands around 509–513 nm. As shown in the figure, the absorption wavelength of the LSPR band changes with the $AgNO_3$ concentration while that of the TSPR band is fixed. For the remainder of the paper, we will designate the two different NRs as Au NRs 634 and Au NRs 819.

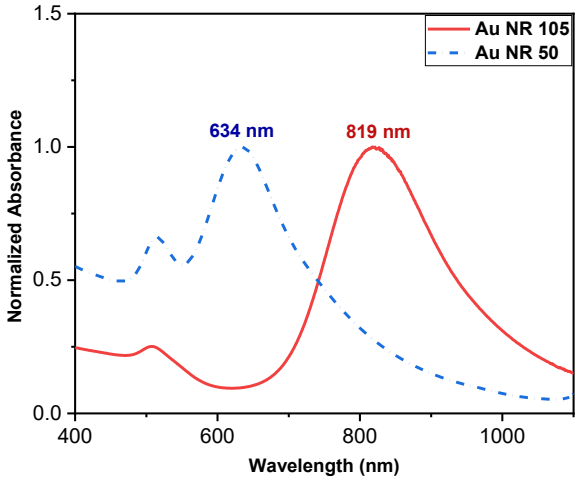

Fig. 1. Normalized absorption spectra of Au NRs prepared with different concentrations of $AgNO_3$ as follows: (a) 50 µM (Au NRs 634), (b) 105 µM (Au NRs 819).

Morphology and dimensions of Au NRs

Fig. 2 displays the TEM images of the prepared Au NRs. Both samples have a nanorod-shaped morphology with few nanosphere particles formed. The high yield of Au NRs is due to the presence of the Ag^+ ions, whose concentration is proportional to the aspect ratio of the Au NRs (Table 1). It is clear from the table that the higher the concentration of Ag^+ the larger is the aspect ratio of the nanorods. From the TEM images, the two aspect ratios of the Au NRs were estimated to be 2.41 and 4.93.

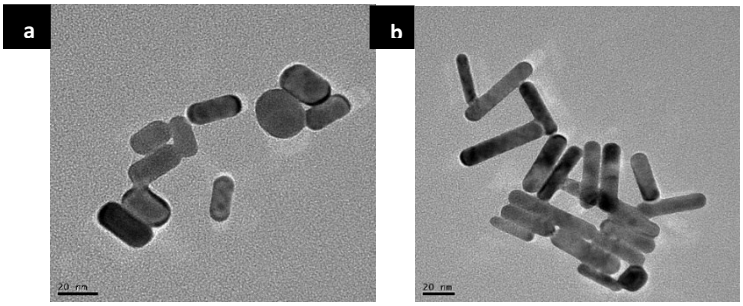

Fig. 2. TEM images of Au NRs with two aspect ratios: (a) Au NRs 634, (b) Au NRs 819.

Table 1. Average aspect ratios, lengths, and widths of the Au NRs.

	Au NRs 634	Au NRs 819
Average width	14.07	10.64
Average length	33.72	51.60
Aspect ratio	2.41	4.93

Elemental composition of Au NRs@TiO_2

The elemental composition of the nanocomposites was confirmed using XPS analysis, which was also used to examine the chemical shifts and the nature of the chemical bonds in the surface region. Fig. 3(a) shows the high-resolution XPS spectra of Ti 2p peaks for TiO_2 and Au NRs@TiO_2. The Ti 2p spectrum for TiO_2 NPs exhibited two peaks at 457.8 eV and 463.6 eV which corresponds to the binding energies of the Ti $2p_{3/2}$ and Ti $2p_{1/2}$ core levels, respectively, due to the presence of the Ti(IV) state [4, 9]. Moreover, the high-resolution spectra of the O 1s energy state for both TiO_2 and the nanocomposite are depicted in Fig. 3(b). The binding energy of the O 1s state for the samples was identified at 529.5 eV, corresponding to the bulk oxides (O^{2-}) within the P25 lattice of TiO_2 [4]. Decorating Au NRs on TiO_2 NPs leads to a blue shift of the Ti 2p and O 1s peaks. This shift is attributed to the interaction between TiO_2 NPs and Au NRs, which suggests that the increased binding energies of Ti 2p and O 1s are due to an electronic charge transfer from TiO_2 NPs to Au NRs. Furthermore, the Au 4f spectrum of the nanocomposite contains two peaks at 82.9 eV and 86.5 eV, representing binding energies of the Au $4f_{7/2}$ and Au $4f_{5/2}$ core levels, respectively. This result indicates the presence of Au in its metallic state [4].

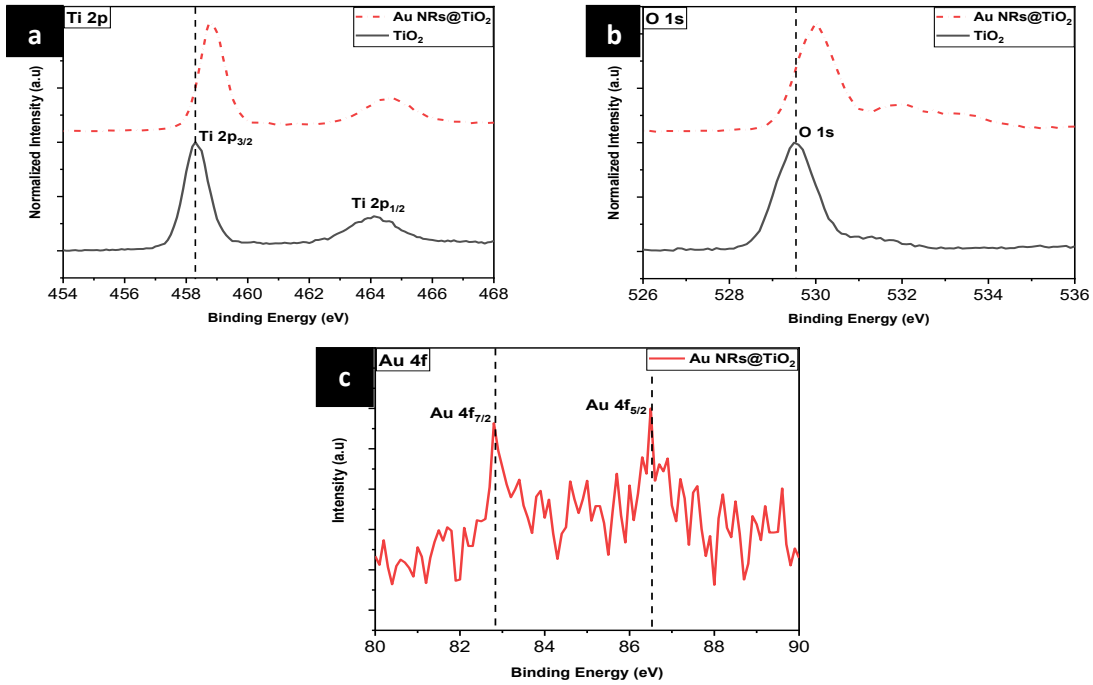

Fig. 3. High resolution XPS spectra: (a) Ti 2p, (b) O 1s, and (c) Au 4f for TiO_2 and Au NRs@TiO_2

.

Photoluminescence of TiO_2 nanoparticles

The PL spectra of TiO_2 NPs decorated with the two different aspect ratios of Au NRs are presented in Fig. 4. The PL spectrum of pristine TiO_2 is included for comparison. Within the 385-530 nm range for Au NR 634@TiO_2 and Au NR 819@TiO_2, five peaks are detected. Among these, a single peak appears in the ultraviolet region at 386 nm (3.21 eV), which is approximately equal to the bandgap energy of TiO_2. In the visible range, the spectrum includes four peaks at 420 nm (2.95 eV), 444 nm (2.79 eV), 483 nm (2.57 eV), and 530 nm (2.34 eV). These visible peaks are caused by defect states in the TiO_2 NPs, which introduce new electron trap energy levels.

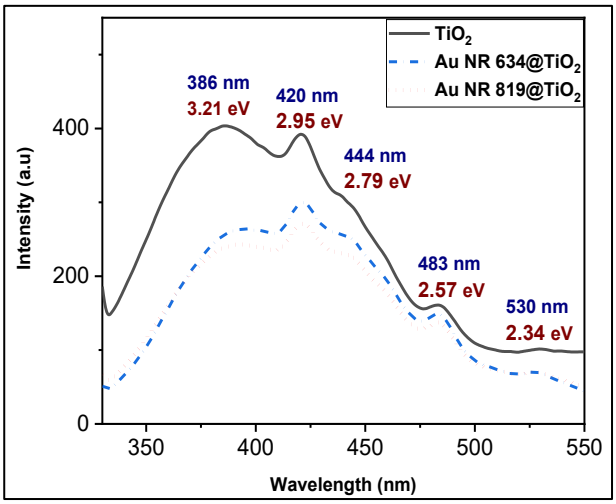

Fig. 4. Photoluminescence spectra of TiO_2 nanoparticles coated with two different aspect ratios of Au NRs. λ_{ex} = 310 nm.

Deposition of Au NRs onto TiO_2 NPs causes significant decrease in the emission intensity. This demonstrates that the efficiency of electron-hole recombination was decreased in TiO_2 NPs coated with Au NRs, which can be attributed to relocation of the excited electrons in the conduction band to the surface of Au NRs, thus reducing electron-hole recombination. This is primarily related to the formation of a Schottky barrier at the contact between Au NRs and TiO_2 that effectively traps the electrons by acting as an electron sink [4, 18-20]. Furthermore, the intensity of the PL peaks of Au NR 819@TiO_2 is lower, compared to that of Au NR 634@TiO_2. This suggests that the larger aspect ratio of Au NRs achieves the highest electron trapping and charge carrier separation along with the lowest rate of electron-hole recombination.

CONCLUSION

This study investigates the utilization of Au NRs to modify the TiO_2 semiconductor nanolayer for potential integration into DSSCs as photoanodes. The objective is to improve absorption in the visible to NIR spectral region and alleviate electron-hole recombination. Two different aspect ratios of Au NRs were synthesized, and their interaction with TiO_2 was examined. Both types of Au NRs exhibit distinct absorption peaks in the visible to NIR spectral range owing to the surface plasmon resonance effect. The aspect ratios of the synthesized Au NRs were determined by transmission electron microscopy. X-ray photoelectron spectroscopy measurements indicated electronic charge transfer from TiO_2 NPs to Au NRs, as evidenced by blue shifts of the Ti 2p and O 1s peaks. PL analysis revealed a decrease in the emission intensity of TiO_2 NPs decorated with Au NRs, as a result of the formation of a Schottky barrier that reduces electron-hole recombination by serving as an electron sink. Remarkably, the PL intensity of TiO_2 NPs decorated with Au NRs of larger aspect ratio (4.93) is lower compared to those decorated with Au NRs of smaller aspect ratio (2.41), suggesting superior electron trapping and charge carrier separation, resulting in reduced electron-hole recombination rates.

Acknowledgement: *The authors would like to acknowledge the financial support provided through the International Research Collaboration Co-Funding Program (IRCC) from Sultan Qaboos University and Qatar University, with Grant reference number CL/SQU-QU/SCI/24/01.*

REFERENCES

1. M. Farzadkia, E. Bazrafshan, A. Esrafili, J. K. Yang, M. Shirzad-Siboni, *J. Env. Health Sci. Eng.*, **13**, 35 (2015).
2. A. A. Kashale, K. P. Gattu, K. Ghule, V. H. Ingole, S. Dhanayat, R. Sharma,J.-Y. Chang, A. V. Ghule, *Compos. B*, **99**, 297 (2016).
3. N. Kunthakudee, T. Puangpetch, P. Ramakul, K. Serivalsatit, M. Hunsom, *Int. J. Hydrogen Energy*, **47**, 23570 (2022).
4. S. P. Lim, Y. S. Lim, A. Pandikumar, H. N. Lim, Y. H. Ng, R. Ramaraj, D. C. S. Bien, O. K. Abou-Zied, N. M. Huang, *Phys. Chem. Chem. Phys.*, **19**, 1395 (2017).
5. L. G. Devi, K. M. Reddy, *Appl. Surf. Sci.*, **257**, 6821 (2011).
6. H. Wei, J.-W. Luo, S.-S. Li, L.-W. Wang, *J. Am. Chem. Soc.*, **138**, 8165 (2016).
7. S. Nakade, Y. Saito, W. Kubo, T. Kitamura, Y. Wada, S. Yanagida, *J. Phys. Chem. B*, **107**, 8607 (2003).

8. P. Roy, D. Kim, K. Lee, E. Spiecker, P. Schmuki, *Nanoscale*, **2** , 45 (2010).
9. S. P. Lim, A. Pandikumar, N. M. Huang, H. N. Lim, *RSC Adv.*, **4**, 38111 (2014).
10. J. M. Macak, F. Schmidt-Stein, P. Schmuki, *Electrochem. Commun.*, **9**, 1783 (2007).
11. T. Ohno, M. Akiyoshi, T. Umebayashi, K. Asai, T. Mitsui, M. Matsumura, *Appl. Catal. A*, **265**, 115 (2004).
12. H. L. Meng, C. Cui, H. L. Shen, D. Y. Liang, Y. Z. Xue, P. G. Li, W. H. Tang, *J. Alloys Comp.*, **527**, 30 (2012).
13. L. Zhang, H. Fu, Y.-F. Zhu, *Adv. Funct. Mater.*, **18**, 2180 (2008).
14. P. S. Chandrasekhar, P. K. Parashar, S. K. Swami, V. Dutta, V. K. Komarala, *Phys. Chem. Chem. Phys.*, **20**, 9651 (2018).
15. L. Feng, Z. Xuan, J. Ma, J. Chen, D. Cui, C. Su, J. Guo, Y. Zhang, *J. Exp. Nanosci.*, **10**, 258 (2015).
16. R. Takahata, S. Yamazoe, K. Koyasu, T. Tsukuda, *J. Am. Chem. Soc.*, **136**, 8489 (2014).
17. Y. Okuno, K. Nishioka, A. Kiya, N. Nakashima, A. Ishibashi, Y. Niidome, *Nanoscale*, **2**, 1489 (2010).
18. J. Yu, L. Yue, S. Liu, B. Huang, X. Zhang, *J. Colloid Interface Sci.*, **334**, 58 (2009).
19. G. Žerjav, M. Roškarič, J. Zavašnik, J. Kovač, A. Pintar, *Appl. Surf. Sci.*, **579**, 152196 (2022).
20. N. Bagheri, J. Hassanzadeh, Z. B. Al-Ruqeishi, N. S. Abdul Manan, H. A. J. Al Lawati, O. K. Abou-Zied, *Phys. Chem. Chem. Phys.*, **25**, 19230 (2023).